Computational study of homogeneous multimetallic cooperative catalysis

Giuseppe Sciortino[1] and Feliu Maseras[1]

Giuseppe Sciortino, ORCID 0000-0001-9657-1788
Feliu Maseras, ORCID 0000-0001-8806-2019
fmaseras@iciq.es

[1] Institute of Chemical Research of Catalonia (ICIQ), The Barcelona Institute of Science and Technology, 43007 Tarragona, Spain.

Abstract

Cooperative multimetallic catalysis is a fascinating field of research further expanding the role of homogeneous catalysis. The simultaneous activation of two substrates or functionalities by different catalytic entities and their subsequent coupling are the responsible for the rate acceleration and selectivity exerted by these systems. The nature of the metal moieties is the responsible of the activation step, while selectivity mainly derives from supramolecular interactions between the substrates and the catalysts, particularly during coupling. The control of both activation and coupling opens the way for the design of new highly selective synthetic routes proceeding in mild conditions. Molecular modelling is becoming nowadays an essential tool in rational design of metal-mediated catalysis. Theoretical models provide fundamental insights on the substrate activation by metals as well as on the interactions between the different catalysts. This can allow the deciphering at the atomic level of the preferential pathways leading to different reaction products. In this contribution, we discuss a series of representative examples of multimetallic cooperative processes described by means of molecular modelling.

(*Cooperative catalysis, synergistic catalysis, dual catalysis, multimetallic catalysis, molecular modelling, computational chemistry, reaction mechanisms*)

1 Introduction

The synthesis of new organic entities entails the formation and breaking of chemical bonds, often an energetically demanding process. To overcome these energy requirements avoiding harsh conditions the use of catalysts became a foundational tool in modern organic chemistry. Among several organic and inorganic catalytic processes, those mediated by homogenous organometallic complexes have been widely employed over the last century. The unique ability of *d*-block metals to form both σ and π coordination bonds opened new synthetic routes such as cross-couplings, C-H and C-C activations or olefin functionalization, otherwise difficult to achieve by pure organocatalysis. Moreover, the electronic properties and steric constraints imposed by the organic ligands were able to drive, regio- and stereoselectivity. However, some processes are still unfeasible when using a single catalyst, and they require further activating agents or pre-functionalization of the substrates. Cooperative catalysis, also known as sinergystic catalysis, could be a solution to these problems

The use of homo and hetero-multimetallic systems have indeed emerged as a promising strategy pushing the frontiers of homogeneous organometallic catalysis. Multimetallic cooperativity is widespread in natural metalloenzymes such as for electron transport in respiratory systems, hydrogen evolution in hydrogenases, reduction of O_2, N_2 or N_2O in nitrogenases, N_2O reductase and cytochrome c oxidase respectively, or CO and CO_2 fixation in dehydrogenases or acetyl-CoA synthase.[1] Despite the many successful examples that have been reported for homo dinuclear systems,[2] the synergy between different metal centers is far from being fully understood. Issues remain concerning redox compatibility or competition between catalytic cycles that often derives in deactivation of the catalyst or in predominance of side reaction pathways.[3] Cooperation of Cu and Pd compounds, generally activating nucleophiles and electrophiles respectively, is among the most explored synergistic organometallic combinations. Moreover, Pd displays a broad compatibility with Ag, Mg, Ru, Au, Rh, and V; while Cu is compatible with Ru, Rh, Fe, Mn, Ni and Re. Other well-known hetero-bimetallic combinations are Rh/Ag, Ru/Ti, Ru/Ag, Au/Fe, Ti/Ni, Ni/Mg or Ni/Zn. For a complete overview of the development in the field the interested reader can refer to the recent reviews by Lee and co-workers in ref. [4]. The key steps of a cooperative catalytic mechanism are the synergistic activation of two different substrates, or functionalities of the same reactant for intramolecular processes, and the coupling reaction between the activated groups. The rational control of these two steps opens new possibility for the design of high-selective synthetic routes proceeding in mild conditions.

Molecular modelling is becoming nowadays an essential tool in rational design of metal-mediated catalysis. Theoretical models supply fundamental insights on the substrate activation by metals as well as on non-bonding interactions ruling the selectivity. In monometallic homogeneous catalysis, there is abundant literature reporting excellent examples of computationally characterized mechanism elucidating the subtle effects behind these phenomena.[5] Coupling reactions, for example, have been extensively studied and its features elucidated in detail. The C-X (where X represents a heteroatom) activation generating an electrophilic carbon moiety, mostly comes from a $2e^-$ oxidative addition to low-valence late

transition metal complexes. Such activation depends on the polarization of the C-X bond that often must be functionalized by a halogen atom. A second reactant containing a nucleophilic carbon gets into the first coordination sphere of the catalyst either by π coordination, as in the case of Heck reaction, or *via* transmetallation for cross-couplings. The final step closing the cycle is a reductive elimination or a migratory insertion for cross-coupling and Heck reaction respectively, followed by β hydride elimination forming the new C-C bond and restoring the reduced catalytically active species. By means of computation, subtle effects governing both regio- and stereo-selectivity associated with the coupling reaction have been deeply understood.[6-8]

In this contribution we will present the main techniques and tools used in the field of computational multimetallic homogenous catalysis, along with a series of representative examples in which, by the integration of experimental and computational data, several hetero-bimetallic synergistic processes have been characterized at the molecular level. To conclude, the main insight drawn by these studies with an outlook to future direction on the field will be briefly discussed.

2 Computation at the service of multimetallic catalysis

Multivariable systems like those involving cooperation between two or more organometallic catalysts require a theory level able to describe electronic rearrangement along the reaction coordinate, fine supramolecular interactions as well as to deal with the conformational changes characteristic of extended systems. Electronic structure methods, especially Density Functional Theory (DFT),[9] have been widely applied to homogenous organometallic catalysis, allowing the prediction of energy differences and a variety of molecular properties with good accuracy.[10] Using DFT, the choice of the functional is a critical aspect, indeed a universal functional describing all the properties of the system is still a chimera, and such choice should be based on previous benchmarks for the specific problem. The hybrid B3LYP, CAM-B3LYP or B97D, the (meta)hybrid GGA M06, the (meta)GGA M06-L and the GGA PBE and BLYP should be mentioned because of their wide use in the field. Moreover, to model stereo and/or regioselective processes standing on non-covalent interactions, accounting for dispersion contribution either as additional D2 or D3 corrections or working with parametrized functionals, has become mandatory.[11, 12] Moreover, the use of dispersion correction assure a good prediction of the entropy change in solution based on the wide applied ideal gas/rigid rotor/harmonic oscillator (IGRRHO) approach implemented in most of the available software.[13] The free energy estimation can be further improved by post-treatment corrections based on either quasi-harmonic schemes or low frequency vibrations scaling factors.[11, 14]

With the increase of the computational power over the last years, DFT methods can treat large systems, over 300 atoms, becoming a robust candidate to deal with multimetallic catalytic systems. However, for fast exploration or when only limited computational resources are available, several approximations can be used to reduce the computational time. The simplest approximation consists in a direct cutback of the total number of atoms, modeling large chemical functionalities as smaller groups. Such modelling requires a wise balance between dimension, chemical properties and supramolecular

effects to avoid altering the course of the reaction. Valuable alternatives are the so called multilevel or hybrid Quantum Mechanics/Molecular Mechanics (QM/MM) methods in which the reactive centers of the system are described at DFT level,[15] while peripheral inert regions are treated under MM formalism.[16] Finally, semiempirical Quantum Mechanical (SQM) methods,[17-19] which apply systematic approximations either to Hartree–Fock or DFT theory, result several orders of magnitude faster than *ab initio*. Among others,[17, 18] recent advances include the development of PM7,[20] and modifications of density functional tight binding (DFTB) methods like GFN-xTB.[19]

Dealing with homogenous catalysis in solution, bulk effects should be included. Models can be based either on explicit or implicit solvation. For explicit solvation, where a large numbers of solvent molecules are introduced, options include QM/MM or SQM-based methods. Continuum implicit solvation models, which may also include some explicit solvent molecules, can be used for pure QM calculations. Among the most popular methods, PCM,[21] SMD[22] and COSMO,[23] based on the Self-Consistent Reaction Field (SCRF),[21] should be mentioned.

In cooperative catalysis, particularly for the coupling process, conformational changes[24] as well as different relative positions of the species forming the supramomolecular aggregates could be critical factors determining the selectivity of the reaction. In this context, statistical methods like classical Molecular Dynamics (MD) are fast and interesting tools for the description of such dynamic phenomena. Classical MDs based on MM force-fields, however, may lack appropriate parameters for metals, especially for coordination and metal-carbon bonds. Specific metal force constants and equilibrium parameters could be derived from QM calculation through several methods and tools like FUERZA,[25] MCPB.py[26] or VFFDT[27] and implemented in classical force-fields. Alternative approaches are *ab initio* MDs (AIMD)[28] in which the force constants are computed on-the-fly using first principles (generally DFT for metal catalysed processes) for each configuration of the trajectory.[29] Two different models are possible: the Born-Oppenheimer (BOMD) and the Car-Parrinello (CPMD).[30] In BOMD the forces are extracted optimizing the wavefunction at each step, while in CPMD the orbitals are treated as classical variables and propagated simultaneously with the particles.[30] Moreover, QM/MM based MDs are also valuable options.[31]

Over the last years several complementary techniques and post-treatment analysis emerged as critical tools in order to completely understand and rationalize the catalytic mechanism. Among them DFT-based micro-kinetics models became fundamental tools reproducing real-time experimental data, providing with additional evidence of the theoretical mechanistic proposal, and giving the possibility to fast evaluate different reaction conditions improving the efficiency of the catalysis.[32] [33] The use of NBO,[34] quantum theory of atoms in molecules (QTAIM),[35] Energy Decomposition Analysis (EDA)[36] [37], localized orbitals and their centroids (CLMO)[38] or principal interacting orbital (PIO),[39, 40] can be also helpful in order to characterize the nature of chemical bonds and their rearrangement during chemical reactions. Finally the popular DFT-based NCIPlot (Non Covalent Interaction Plot)[41]

must be mentioned for its capability to characterize intra- and inter-molecular non covalent interactions which are often the base of selectivity.

3 Applications to representative systems

This section is devoted to present the power of computation in this field through a series of recent examples of Rh-M (M=Cu, Ag), Ru-M (M=Cu, Ag), Pd-M (M=Ag, Cu, Mg), V-Pd, Au-Au and Ni-Mg hetero-bimetallic systems, for which the complete cooperation between the two metal moieties has been demonstrated and fully understood. The presented case study are mainly two-electron redox processes based on oxidative addition (OA) and reductive elimination (RE) steps in which Cu, Ag or Mg are used as oxidants. However, other cooperative mechanisms are also possible as briefly presented in section 3.4.

3.1 Rh-M cooperative systems (M=Cu, Ag)

Our group,[42] by means of DFT simulations, shed light on the cooperative oxidative coupling of benzoic acid and alkynes mediated by [Cp*$Rh^{III}(OAc)_2$] (Cp = cyclopentadienyl) in presence of either [$Cu(OAc)_2(H_2O)$] or [Ag(OAc)] as terminal oxidants. In contrast to the previously described cross-coupling mechanisms, in oxidative-coupling the catalyst oxidizes the substrates activating both C-H or X-H functionalities leading to the formation of a new C-C or C-X bond. One of the main features of oxidative coupling is that a stoichiometric amount of an external oxidant is required for the regeneration of the catalytically active species which can allow the subsequent cycle to proceed.

We first discuss the mechanistic overview of the oxidative coupling of benzoic acid and 1-phenyl-1-propyne to form 4-methyl-3phenyl-isocoumarin (Scheme 1a).

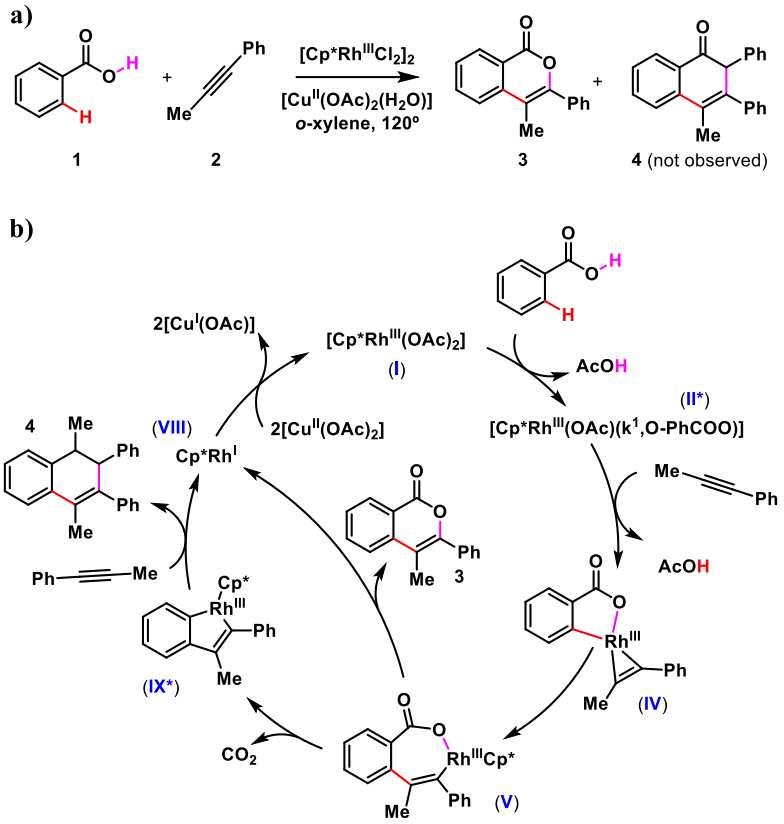

Scheme 1 Scheme of: a) oxidative coupling of benzoic acid and 1-phenyl-1-propyne to form isocumarin;[43, 44] and b) experimentally proposed alternative catalytic cycles.[45] Some steps have been omitted for clarity.

The general mechanism starts with the formation of the [Cp*Rh^{III}(OAc)$_2$] active catalyst that exchanges one acetate by benzoate leading to the [Cp*Rh^{III}(OAc)(PhCOO)] intermediate **I**. In this species, the ortho C-H bond is activated via concerted metalation deprotonation (CMD) assisted by the coordinated AcO^- that in its turn is replaced by η^2 coordination of the alkyne leading to [Cp*Rh^{III}(κ^2*o*C,O- PhCOO)(η^2-Me≡Ph)] intermediate **III**. After a conformational rearrangement the alkyne insertion into the Rh-C bond leads to the Rh^{III} 7-membered rhodacycle **V**. From intermediate **V** a bifurcation was predicted. One possible path goes through CO_2 extrusion leading to a 7-membered rhodacycle **IX** that through another alkyne insertion followed by reductive elimination releases derivative **4**. The other possible path goes through a reductive elimination in rhodacycle **V** generating the isocumarin, **3**, which is the only product observed experimentally. Both pathways form a Cp*Rh^{I} moiety that needs to be reoxidized to Rh^{III} by action of the external copper(II) acetate closing the catalytic cycle (Scheme 1b).

Based on this general mechanism, two major reaction schemes could be drawn: i) two separated pathways with independent reductive elimination steps and subsequent reoxidation; ii) or a single cycle involving the formation of a supramolecular aggregate in which both metal moieties cooperate in the reductive-elimination process. By a full DFT exploration of the potential energy surface (PES) based on the

simplified [$CpRh^{III}(OAc)_2$] catalyst, the cycle modelled considering independent metal moieties leads preferentially to the naphthalene derivative **4**. The activation barrier leading to this derivative is lower by ~5 kcal·mol^{-1} with respect to that going to the isocumarin **3** ($\mathbf{TS_{V\text{-}IX}}$ vs $\mathbf{TS_{V\text{-}VIII}}$). In contrast, the experimentally observed chemoselectivity toward isocumarin was reproduced by modelling the process through the formation of a supramolecular aggregate of Rh^{III} and Cu^{II} moieties (Fig. 1a).

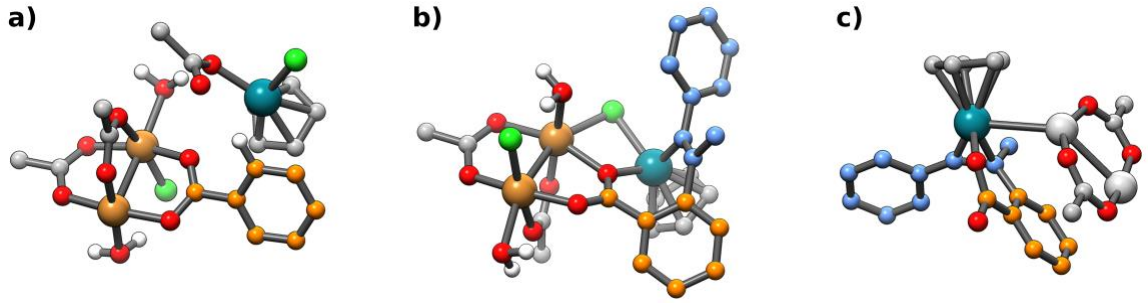

Fig. 1 B97D optimized structure of: a) supramolecular adduct between [Cl_2CpRh^{III}] and [$Cu^{II}_2(OAc)_2(H_2O)_2$] (Intermediate **II**); b) 7-membered rhodacycle coming from alkyne insertion with [$ClCu^{II}_2(OAc)_2(H_2O)_2$] displaying the Cu^{II}-OOCPh coordination hindering the CO_2 extrusion; and c) the 6-membered rhodacycle rhodacycle coming from alkyne insertion and [$Ag^{I}_2(OAc)_2$] with the CO_2 functionality free to be released. 1-phenyl-1-propyne backbone is shown in orange while the benzoate one in blue

This pathway displays a global energy gain ~15 kcal·mol^{-1} arising from the formation of the supramolecular aggregate in solution from which the reaction proceeds selectively toward isocumarin. The key step of the computed synergistic mechanism is the two-step cooperative reductive-elimination (CRE) in rhodacycle trimetallic aggregate of Cp^*Rh^{III} moiey and [$Cu^{II}(OAc)_2(H_2O)]_2$ (Fig. 1b). During the new C-O bond formation two electrons from the organic moiety are separately transferred toward Rh^{III} and Cu^{II} centers generating a Rh^{II}-Cu^{I}-Cu^{II} system. After the isocumarin is released, the trimetallic aggregate rearranges with a further one-electron-transfer from Rh^{II} to the second Cu^{II} center mediated by the chloride bridge, thus regenerating the Rh^{III} catalyst and forming the [$Cu^{I}(OAc)(H_2O)]_2$ waste product (Scheme 2).

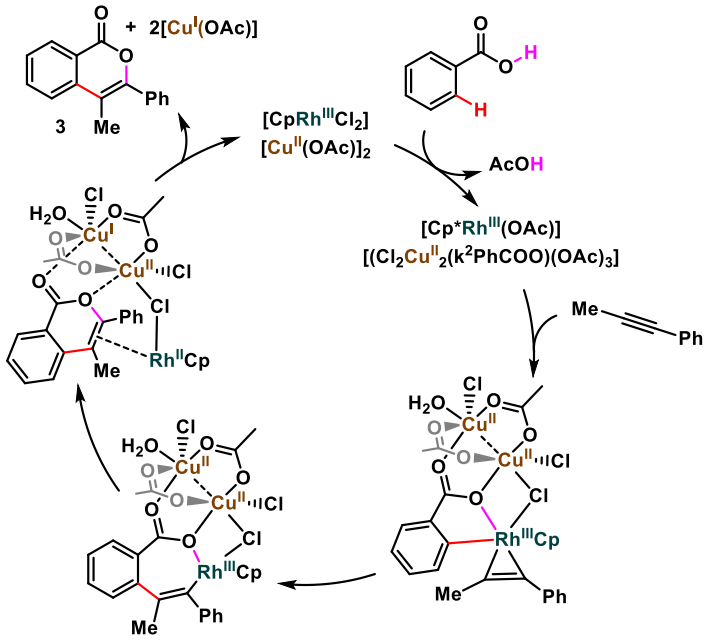

Scheme 2 Simplified cooperative catalytic cycle computed for the oxidative coupling of benzoic acid and 1-phenyl-1-propyne to form isocumarin. For clarity, only the discussed species are depicted, for the complete cycle the interested readers can refers to the original publication in ref. [45]

The origin of the selectivity was found in the interaction of the carboxylate functionality of benzoic acetate with the dinuclear Cu^{II} moiety hindering the CO_2 extrusion (Fig. 1b).

The key role of supramolecular aggregates in solution in this synergistic multimetallic processes was further highlighted in a subsequent work in which the chemo- and regioselectivity of a related reaction was correlated with the nature of the terminal oxidant $[Cu^{II}(OAc)_2(H_2O)]$ or $[Ag^{I}(OAc)]$ (Scheme 3).[46]

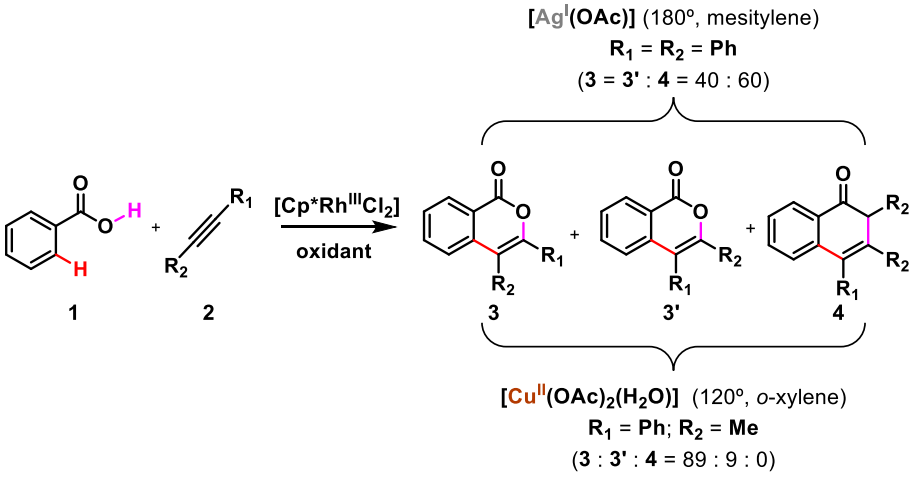

Scheme 3 Oxidative coupling of benzoic acid and alkyne with different oxidants ([$Cu^{II}(OAc)_2(H_2O)$] or [$Ag^{I}(OAc)$]) to form 4-methyl-3-phenyl-isocumarin (**3**), 4-phenyl-3-methyl-isocumarin (**3'**), and a naphthalene derivative (**4**) [46]

The origin of the regioselectivity toward isocumarin, **3** (**3** : **3'** = 89 : 9, see Scheme 3) has been ascribed to the relative orientation of the Me substituent of 1-phenyl-1-propyne during the alkyne insertion corresponding to $\mathbf{TS_{IV\text{-}V}}$ of Scheme 1. The transition state with the Me oriented toward benzoate ring was favored by ~2.5 kcal·mol^{-1} in agreement with the experimental selectivity of ~90%. Furthermore, calculations also explained why the use of [$Ag^{I}(OAc)$] as oxidant destroyed the chemoselectivity toward isocumarin giving a mainly racemic mixture of **3** and **4** (40:60, see Scheme 3). The hindrance toward CO_2 extrusion exerted by COO^- coordination to copper described above (Fig. 1b) is prevented by using silver(I) acetate (Fig. 1c) leading to mainly isoenergetic pathways for the formation of the isocumarin and naphthalene derivatives.

The examples in this section showcase the power of molecular modelling for the understanding of multivariable systems like cooperative processes, and highlight the potential role of aggregation in solution.

3.2 Ru-M cooperative systems (M=Cu, Ag)

In 2018, in a collaboration with the experimental group of Patureau, we reported a complete mechanistic study on a Ru/Cu co-catalyzed dehydrogenative homo-coupling of two carbazoles to form C-N bridged bicarbazoles (Scheme 4).[46]

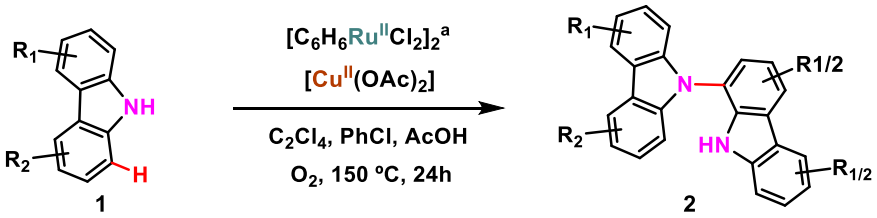

Scheme 4 Scheme of the dehydrogenative homo-coupling of carbazoles to form C-N bridged bicarbazoles co-catalyzed by Ru^{II} and [$Cu^{II}(OAc)_2$] catalysts. Among the eleven different Ru^{II} catalyst synthesized only [$C_6H_6Ru^{II}Cl_2]_2$ is reported, as it was the one computationally modelled.

The PES was explored within the framework of DFT and SMD continuum approximation for diphenylether (ε=3.73) modelling the effects of the solvent mixture used in the experimental reaction (PhCl, ε=5.70 and C_2Cl_4, ε=2.27). The [$C_6H_6Ru^{II}(Cl)_2]_2$ catalyst was used as the most simple complex catalyzing the reaction, while the dimeric copper acetate was used as the thermodynamically most stable form of the co-catalyst. The integrated kinetic and theoretical study unearthed a cooperative mechanism proceeding through the formation of a supramolecular aggregate in solution involving both Ru and Cu moieties (see Fig. 2).

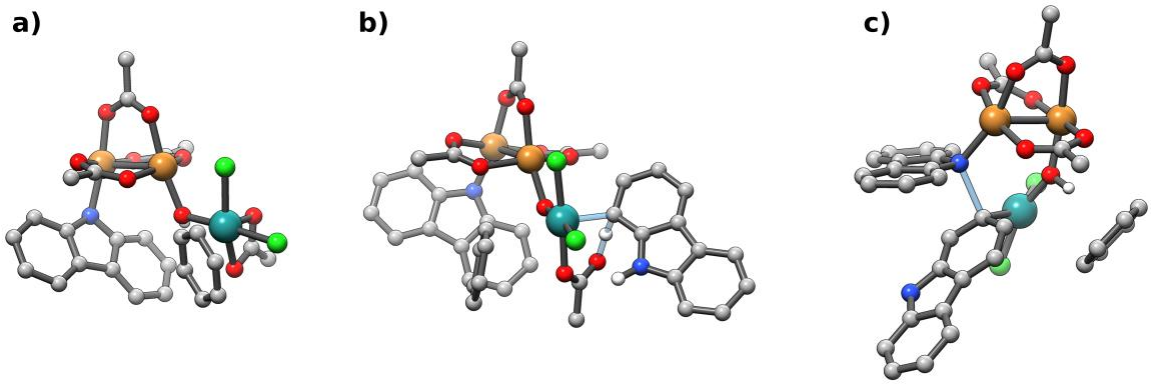

Fig. 2 B97D optimized structure of trimetallic species: a) O-bridged Ru^{III}-O-Cu^{II}-Cu^{II} intermediate; b) transition state for C-H activation via Ru^{III}-mediated concerted metalation deprotonation; and c) transition state for C-N bond formation through $1e^-$ cooperative reductive elimination. Bonds formed and broken in TSs are depicted as transparent sticks

The cycle, reported in Scheme 5, starts with an oxidative N-H activation of the carbazole by copper diacetate in which the hydrogen and one electron are transferred to one Cu^{II} center and one acetate ligand. After conversion of $[C_6H_6Ru^{II}(Cl)_2]_2$ by dioxygen in its Ru-oxyl active species $[C_6H_6Ru^{III}OCl]$, a trinuclear O-bridged Ru^{III}-O-Cu^{II}-Cu^{II} species is formed by coupling the Cu^{I} moiety with the Ru-based oxyl radical (Figure 2a). From this trimetallic aggregate, a Ru^{III}-mediated CMD is invoked for the C-H activation of a second carbazole. In this step the leaving proton is transferred to the Ru-coordinated acetate (TS2 in Figure 2b). It must be highlighted that monometallic alternative for the C-H activation led to high energy demanding pathways, that were consequently discarded. The final step is a cooperative reductive elimination, which is subtly different from that discussed above for the Rh/Cu system. In this case, the coupling involves a nitrogen with radical character, thus a single C to Ru electron transfer occurs during the formation of the new C-N bond with the concerted reduction of Ru^{III} to Ru^{II} (TS2 in Figure 2c). Finally, the cycle is closed by regeneration of the catalyst and expulsion of a water molecule as byproduct.

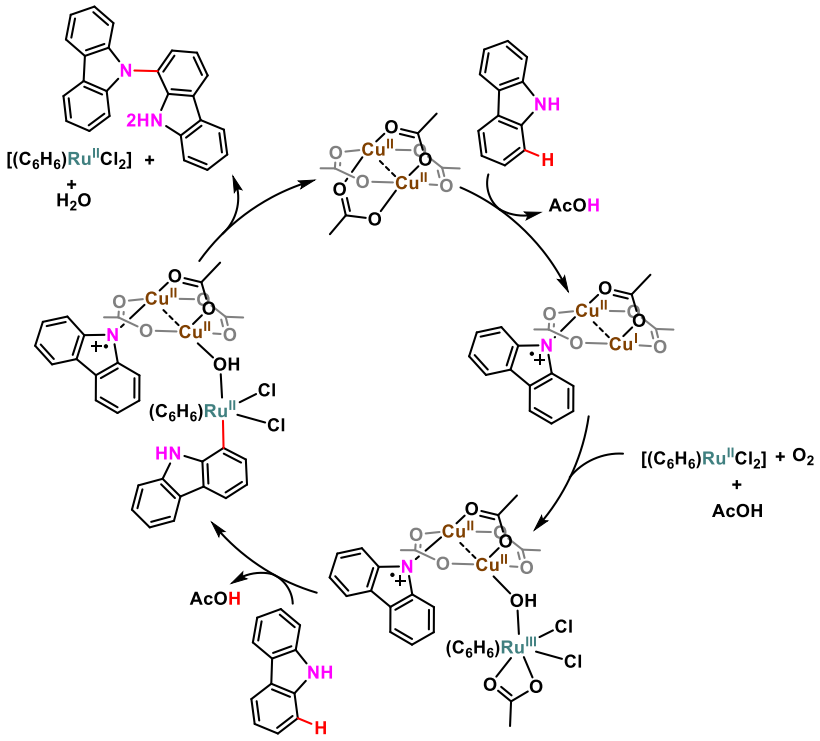

Scheme 5 B97D computed cycle for the dehydrogenative homo-coupling of carbazoles to form bicarbazoles co-catalyzed by $[PhRu^{II}Cl_2]^2$ and $[Cu^{II}(OAc)_2(OH_2)]_2$. Only the discussed steps are depicted for clarity

The computed cooperative mechanism accounts for the kinetic order of the reaction suggesting the formation of polymetallic Ru/Cu (1:2) aggregates in the rate-determining step identified as the CRE. In the same work, the authors also analyzed the complete regioselectivity of the process toward N-C1 bond formation. The kinetic barriers obtained for CRE are in line with this finding showing an activation energy order in kcal·mol^{-1} of C1 3.7< C3 2.7< C2, consistent with a 99% selectivity.

Results in this second section confirm the relevance of aggregates in solution for cooperative catalysis.

3.3 Pd-M cooperative systems (M=Ag, Cu, Mg)

The Sonogashira reaction is a widely used cross-coupling process. Generally, it requires the synergistic cooperation between a Pd^0 catalyst and a Cu^I-based co-catalyst and its accepted mechanism follows the steps described above for general cross-couplings, namely oxidative addition at the Pd^0 moiety, transmetalation and reductive elimination.

Khusnutdinova, Lledós and co-workers[47] recently published an integrated experimental/computational mechanistic study of the cooperative transmetallation and reductive elimination steps occurring in a Sonogashira coupling. The work was triggered by the experimental isolation and complete structural characterization of a series of tri and tetra-nuclear hetero-bimetallic

Pd^{II}_2(aryl)-Cu^{I}_n (n=1 or 2) complexes serving as a functional model for the intermediates coming from oxidative addition of benzo[h]quinolone, BzhQ (Scheme 6a and b). The steps under analysis were the formation of the Pd^{II}(aryl/acetilyl)-Cu^{I}_n by CMD of 4–ethynylanisole over the Pd^{II}_2(aryl)-Cu^{I}_n assemblies and the subsequent C-C coupling between the terminal alkyne and aryl moieties (Scheme 6c and d).

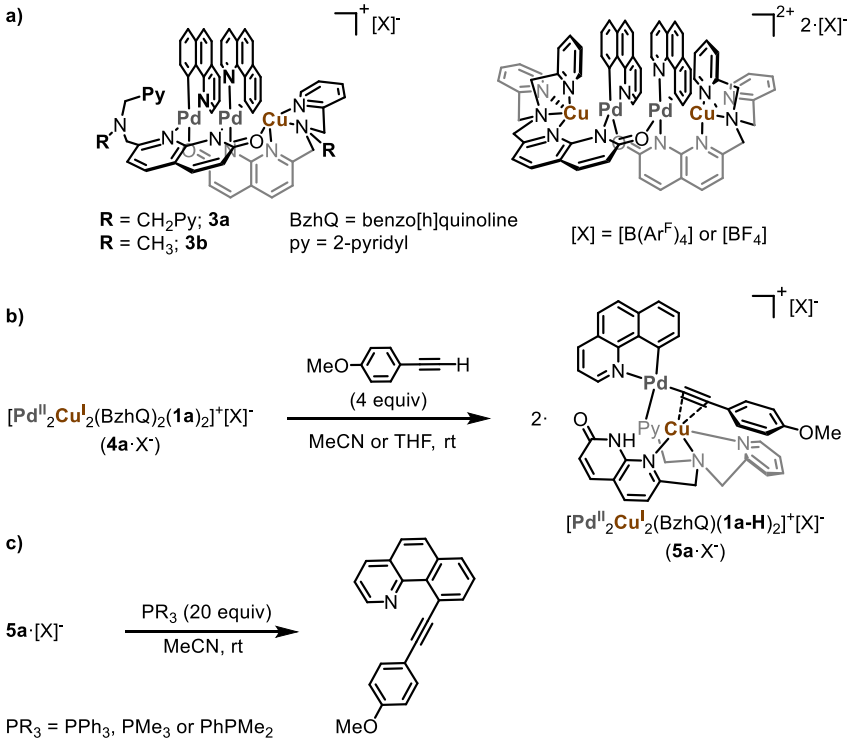

Scheme 6 Species involved in the Sonogashira reaction. a) tri and tetranuclear synthesized models; b) transmetallation reaction; and c) reductive elimination. Among the four characterized complexes only the reactive species are reported

The reactivity of the synthesized tri- and tetra-nuclear compounds toward terminal alkyne activation depends significantly on the Pd···Cu interatomic distance. Indeed, only assemblies featuring Pd···Cu distances about 2.66(1) Å enabled activating terminal alkyne. Moreover, no reaction was observed using a system consisting of a Cu^{I} monomer plus the [Pd^{II}_2(BzhQ)$_2$(OAc)$_2$] dimer, which further highlights the importance of Pd/Cu association in this process. Further reactivity attempts on the C-C bond reductive elimination mediated by Pd^{II}-Pd^{II}(aryl/acetilyl)-Cu^{I}_2 pointed out the formation of the coupling product with high yields only in presence of phosphine additives commonly used in Sonogashira reactions. Based on these observations, the authors reported a reaction mechanism for the most active assembly by applying a multi-step computational strategy involving static DFT calculations in implicit solvent to characterize minima and transition states, and DFT-based AIMDs in gas phase combined with metadynamics to explore the wide conformational changes along the reaction coordinate.

The first step of the reaction is a ligand exchange over the Cu^{I} center in which one pyridyl group is replaced by η^2 coordination of the alkyne (Scheme 7, I1). The Cu^{I}-acetylide intermediate is formed by a low barrier pyridyl-assisted CMD step (Scheme 7, I1-I3). The resulting intermediate cannot undergo transmetallation yet, as it needs a global conformational change to bring the Pd^{II} center closer to the triple bond in order to form a σ-Cu^{I},π-Pd^{II}–alkyne species. This movement was analyzed by *ab initio* metadynamics disclosing a low cost coordination rearrangement in which the N_{Naph} donor, originally bound to Pd^{II}, is transferred to Cu^{I} with the concerted π-coordination of the acetylide moiety entailing a switch from linear (~170º) to triangular (~65º) disposition of $Cu^{I}\cdots Pd^{II}\cdots Pd^{II}$ nuclei (Scheme 7, I3-I4). From this intermediate, the acetylide transmetallation occurs *via* a low energy bending of the triple bond interconverting from σ-Cu^{I},π-Pd^{II}–alkyne to σ-Pd^{II},π-Cu^{I}–alkyne (Scheme 7, I4-I5). The electronic rearrangement of this key step was further clarified by following the centroids of the localized molecular orbitals along the reaction coordinate. From **I5**, a proton transfer entailing the coordination of Cu^{I} by N_{py} gives **I6**. This transformation requirew a further conformational change, assessed by meta AIMDs, in order to separate the Pd^{II} and Cu^{I} moieties (Scheme 7, I6-I7), followed by two additional proton transfer (Scheme 7, I7-I9). A final coordination rearrangement in which the carbonyl is substituted by the dangling N_{py} donor on the Pd^{I} center leads to the dissociation of the tetranuclear cluster giving [Pd^{II}(**1a-H**)Cu^{I}(BzhQ)]$^+$ and [σ-Pd^{II},π-Cu^{I}–alkyne(**1a-H**)(BzhQ]$^+$ in which the aryl and acetylide ligands are arranged cis to each other, Scheme 7, I9-(PdCu+5a).

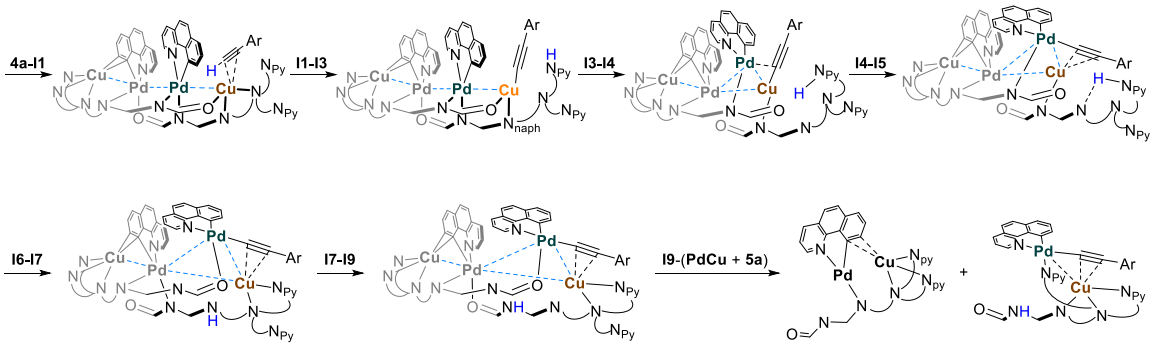

Scheme 7 Schematic representation of the main intermediates computed for the reaction mechanism leading to the formation of **5a** from **4a** and 4-ethynylanisole. Only the discussed species are depicted for clarity. Catalytic cycle computed at B3LYP-D3 theory level

Reductive elimination assisted by PMe_3 over the [σ-Pd^{II},π-Cu^{I}–alkyne(**1a-H**)(BzhQ]$^+$ intermediate was also studied disclosing three main steps, PMe_3 coordination at the Pd^{II}-acetilyde center, [Cu^{I}(**1a-H**)(PMe_3)]$^+$ elimination, and reductive coupling.

This representative case highlights several factors that ought to be taken into account when modelling a multimetallic process: i) coordination and electronic rearrangements; ii) intermetallic

distances; iii) and the dynamic flexibility of the multimetallic assemblies favoring the abovementioned transformations.

In the same context, we explored the trifluoromethylation mediated by the cooperative action of Ag^{I} additive, in a collaboration with the experimental group of Pérez-Temprano (Scheme 8a).[48]

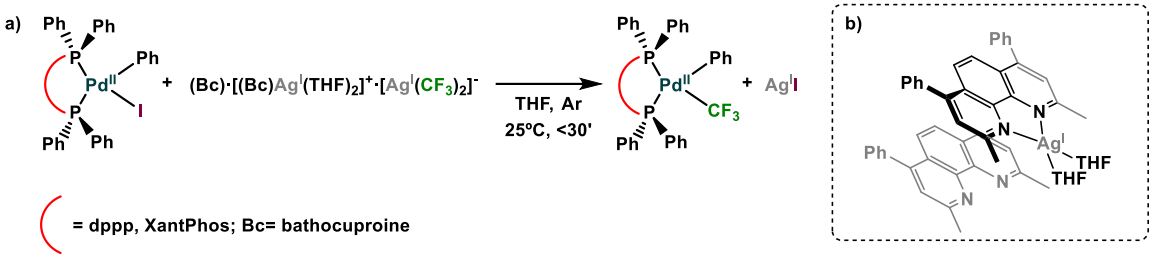

Scheme 8 a) Scheme of the trifluoromethylation cooperative transmetallation step mediated by Ag^{I} additive. b) Molecular structure of the active species of the Ag^{I} additive. Simulations carried out at ωB97-xD DFT theory level.

Similarly to the previous case the key step of the processes is the cooperative additive-mediated transmetallation reaction. The hard work here consisted in the characterization of the active species of the co-catalyst through a joint experimental/DFT study. ^{1}H DOSY NMR experiments excluded the species $[(Bc)_2Ag^{I}]^{+}$ as the countercation of the $[Ag^{I}(CF_3)_2]^{-}$. Full DFT simulations supported by XRD analysis unveiled the most stable partner of the trifluoromethylsilver(I) anion as the square pyramidal $[BcAg^{I}(THF)_2]^{+}$ including a further Bc ligand in the second coordination sphere interacting by π-stacking (Scheme 8b).

In 2019 Dang and co-workers,[49] by a combination of experimental and DFT analyses reported the cooperative $[Pd^{II}(OAc)_2]$−glyoxylic acid mechanism, for the γ-C(sp^3)−H arylation of aliphatic amines, in presence of the Ag^{I}TFA additive Scheme 9a.

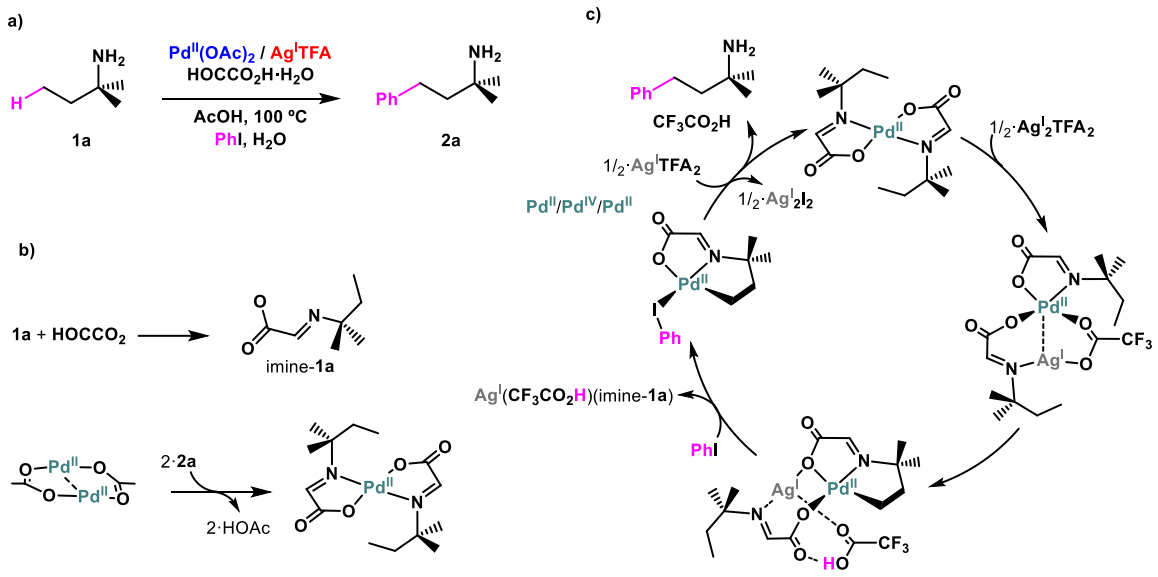

Scheme 9 a) Scheme of the γ-C(sp^3)−H arylation of aliphatic amines catalyzed by [$Pd^{II}(OAc)_2$] and AgITFA co-catalyst. b) Active catalyst generation. c) Mechanism outline of the cooperative process. Only the discussed species are depicted for clarity. Catalytic cycle computed at BP86-D3(BJ) DFT theory level.

The active catalyst [Pd^{II}(imine-**1a**)$_2$] had been isolated and characterized by X-ray diffraction as the Pd^{II} bischelated complex of iminoacetic acid imine-**1a** coming from the condensation reaction of amine **1a** and glyoxylic acid (Scheme 9b). The general reaction mechanism consists in three main steps: C−H activation by concerted metalation deprotonation, oxidative addition of PhI, and C−C reductive elimination/coupling. The carboxylate-assisted CMD was computed in absence of silver trifluoroacetate, and gave activation barriers for the ranging from 30 up to 37 kcal·mol^{-1}. When considering the formation of a [Pd^{II}(imine-**1a**)$_2$]·1/2[$Ag^I_2(CF^3CO_2)_2$] supramolecular adduct, the barrier for Ag^ITFA assisted CMD was lowered by ~5 kcal·mol^{-1}. The supramolecular aggregation of the Pd-Ag dinuclear species was also confirmed by matrix-assisted laser desorption-ionization time-of-flight mass spectrometry (MALDI-TOF MS). The cyclometallated species undergoes to substitution of PhI and through oxidative addition forms a penta-coordinated [Pd^{IV}I(Ph)(H_{-1}imine-**1a**)]. The following step is the iodine abstraction by $Ag^I(CF^3CO_2)$ moiety giving rise a hexa-coordinated [$Pd^{IV}(\kappa^2$-CF^3CO_2)(Ph)(H_{-1}imine-**1a**)] from which C-C reductive elimination/coupling leads substrate arylation regenerating the Pd^{II} species (Scheme 9c).

In 2020 Tomson, Walsh and co-workers reported a DFT exploration of Pd-catalyzed Kumada−Tamao−Corriu (KTC) cross-coupling of aryl Grignard reagents to fluoroarenes highlighting its Pd^{II}/Ag^I bimetallic cooperative mechanism (Scheme 10a).[50]

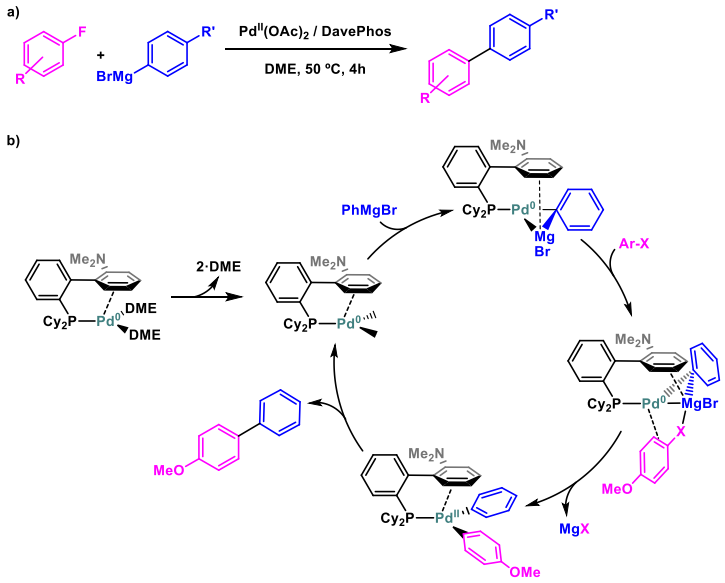

Scheme 10 a) Scheme of the Pd-catalyzed Kumada−Tamao−Corriu (KTC) cross-coupling of aryl Grignards to fluoroarenes b) Mechanism outline of the cooperative process. Catalytic cycle computed at B97-D3 DFT theory level. Only the discussed species are depicted for clarity

.

Their results further support a previous mechanistic proposal by Nakamura *et al.*[51] [52] where the Mg ion is directly involved in the oxidative addition of the C−F bonds in Ni-based related processes. Competition experiments using 1:1 mixture of chloro- and fluoroarenes varying the amounts of PhMgBr pointed out that only at a high Mg/ArX ratio (2.5:1) the activation of Ar-F become competitive with the Ar-Cl activation suggesting two different pathways depending on the metal ratio. The authors compared both mono- and bimetallic pathways for the KTC cross-coupling of ArX (X=Cl or Br) with PhMgBr catalyzed by Pd^0(DavePhos) monophosphine complex by means of DFT simulations. As a result, the ArCl oxidative addition is favored by ~15 kcal·mol^{-1} following a monometallic pathway, while the gap is reduced to ~1 kcal·mol^{-1} including Mg ion in the simulation. The complete computed mechanism starts with the association of Pd^0(DavePhos) with PhMgBr that through a low barrier conformational rearrangements establishes a Pd-ArX π-interaction preparing the subsequent C-X bond breaking (Scheme 10b). The following hetero-bimetallic transition state for the oxidative addition is driven by simultaneous Pd backbonding to the arene and Mg-mediated activation of the halide. The cooperative pathway was finally assessed by using sterically inhered aryl halides that notably influenced the yield of the reaction supporting the hetero-bimetallic nature of the process.

Sunoj and co-workers[53] in 2020 further investigated the role of a silver additive in Pd catalyzed aryl C-H activation in phosphorylation, arylation, alkynylation, and oxidative cycloaddition reactions using a full DFT approach (Scheme 11a).

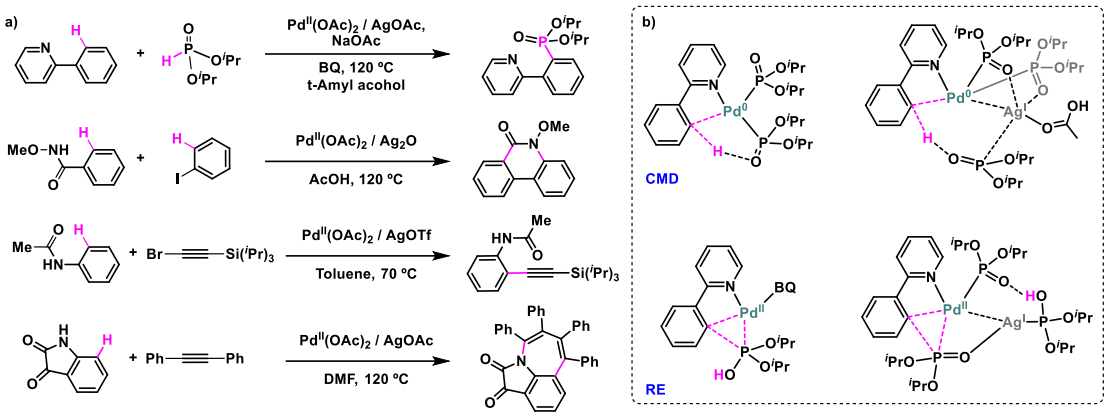

Scheme 11 a) Scheme of the Pd-catalyzed C-H activations analyzed. b) Scheme of the mono and bimetallic CMD and RE transition states for the phosphorylation reaction. Catalytic cycle computed at M06 DFT theory level

By a systematic investigation of the relative barriers for mono- and hetero-bimetallic CMD and RE steps the clear tendency of explicit silver salts to reduce both energy spans were assessed providing additional evidences for the formation of Pd-Ag multimetallic aggregates in solution. The complete mechanistic pathways were computed unveiling the active role of Ag in lowering both CMD and RE transition states. In CMD, silver additives reduce the steric strain during the proton transfer as well as increase the polarization of the C-H through Pd-Ag electron communication as shown by structural and MO analyses (Scheme 11b). The Pd-Ag electron communication has been found to be also the driving force in the reductive elimination step (Scheme 11b).

All the works reported in this section further highlight the necessity to explicitly include the metal-additives in order to reproduce and predict multimetallic processes.

3.4 Other cooperative processes

Bimetallic cooperative processes have been recently computationally assessed for serval mono and hetero-bimetallic systems involving among others V, Au, or Ni. Dinuclear catalysts have been also explored, however this topic is out of the scope of the present review.[54-59]

Himo and co-workers[60] in 2017 by means of DFT and microkinetics explored the V-Pd cooperative mechanism of the combined Meyer−Schuster rearrangement/Tsuji−Trost allylic substitution between propargylic alcohols and allylic carbonate. In contrast with the cases reported above, this work established two independent catalytic cycles, the V-catalyzed rearrangement and the Pd-mediated O-allylation, crossing in a bimetallic coupling pathway.

In 2019, Hyland, Pyne and co-workers[61] reported the Au-catalyzed cycloaromatization of isoindolines and through DFT simulation a dual gold mechanism has been established. The central step of the process is the formation of a σ,π gold dinuclear complex in which the enyne moiety is by activated

toward intramolecular nucleophilic attack of the gold-acetylide by π coordination of an additional LAu^+ unity.

In the framework of bimetallic Ni catalyzed processes, two works of 2005 and 2009 by Nakamura and co-workers,[51, 52] reported a bimetallic mechanistic proposal of Ni-hydroxyphospine coupling of aryl electrophiles and Grignard reagents. As discussed for the case of Pd^0(DavePhos) (Scheme 10) the hetero-bimetallic transition state for the OA is driven by synergistic action of Ni backbonding to the arene and Mg-activation of the halide.

4 Conclusions and future directions

The series of examples presented in this contribution highlights the power of computational chemistry to handle multivariable cooperative processes. In particular, they show how the formation of supramolecular aggregates in solution, an aspect often overlooked, can play a pivotal role in the reproduction and prediction of multimetallic cooperative catalysis. Moreover, several aspects emerge as relevant factors in cooperative homogeneous catalysis: i) coordination and electronic rearrangements; ii) intermetallic distances; and iii) dynamic flexibility of the multimetallic assemblies.

The main challenge for an increased application of calculations to this field is the intrinsic complexity of the problems: large supramolecular aggregates with conformational flexibility; subtle metal-substrate interactions; complex reaction networks; and potentially important roles for solvent molecules and counter-ions. In view of this, the complementary application of different theory levels and techniques, such as QM, MM and MDs seems appropriate, either as a multistep combination or as a multiscale method. Automated exploration tools to investigate the conformational space and reactivity of supramolecular aggregates is also an interesting option.

In summary, the application of computational chemistry in the field of cooperative catalysis is still in its early stages, but it holds large promise, as calculation is likely to play an increased role in the development of this exciting field of research.

Acknowledgements

We thank for financial support the CERCA Programme/Generalitat de Catalunya and MINECO (Grant PID2020-112825RB-I00). G.S. thanks Spanish MINECO Juan de la Cierva program, FJC2019-039135-I. Prof. Agustí Lledós is kindly acknowledged for fruitful discussions.

Conflict of interest

The authors do not have conflicts of interest to declare.

References

1. Ghosh, A. C.; Duboc, C.; Gennari, M., (2021) Synergy between metals for small molecule activation: Enzymes and bio-inspired complexes. Coord. Chem. Rev. 428:213606. https://https://doi.org/10.1016/j.ccr.2020.213606
2. Campos, J., (2020) Bimetallic cooperation across the periodic table. Nature Reviews Chemistry 4:(12)696-702. https://10.1038/s41570-020-00226-5
3. Romiti, F.; del Pozo, J.; Paioti, P. H. S.; Gonsales, S. A.; Li, X.; Hartrampf, F. W. W.; Hoveyda, A. H., (2019) Different Strategies for Designing Dual-Catalytic Enantioselective Processes: From Fully Cooperative to Non-cooperative Systems. J. Am. Chem. Soc. 141:(45)17952-17961. https://10.1021/jacs.9b05464
4. Kim, U. B.; Jung, D. J.; Jeon, H. J.; Rathwell, K.; Lee, S.-g., (2020) Synergistic Dual Transition Metal Catalysis. Chem. Rev. 120:(24)13382-13433. https://10.1021/acs.chemrev.0c00245
5. Sperger, T.; Sanhueza, I. A.; Kalvet, I.; Schoenebeck, F., (2015) Computational Studies of Synthetically Relevant Homogeneous Organometallic Catalysis Involving Ni, Pd, Ir, and Rh: An Overview of Commonly Employed DFT Methods and Mechanistic Insights. Chem. Rev. 115:(17)9532-9586. https://10.1021/acs.chemrev.5b00163
6. Sameera, W. M. C.; Maseras, F., (2012) Transition metal catalysis by density functional theory and density functional theory/molecular mechanics. WIREs Comput. Mol. Sci. 2:(3)375-385. https://https://doi.org/10.1002/wcms.1092
7. Harvey, J. N.; Himo, F.; Maseras, F.; Perrin, L., (2019) Scope and Challenge of Computational Methods for Studying Mechanism and Reactivity in Homogeneous Catalysis. ACS Catal. 9:(8)6803-6813. https://10.1021/acscatal.9b01537
8. Lledós, A., Computational Organometallic Catalysis: Where We Are, Where We Are Going. Eur. J. Inorg. Chem. n/a:(n/a)https://https://doi.org/10.1002/ejic.202100330
9. Koch, W.; Holthausen, M. C., *A chemist's guide to density functional theory*. John Wiley & Sons: 2015.
10. Hohenberg, P.; Kohn, W., (1964) Inhomogeneous Electron Gas. Physical Review 136:(3B)B864-B871. https://10.1103/PhysRev.136.B864
11. Grimme, S., (2012) Supramolecular Binding Thermodynamics by Dispersion-Corrected Density Functional Theory. Chem. Eur. J. 18:(32)9955-9964. https://https://doi.org/10.1002/chem.201200497
12. Grimme, S.; Antony, J.; Ehrlich, S.; Krieg, H., (2010) A consistent and accurate ab initio parametrization of density functional dispersion correction (DFT-D) for the 94 elements H-Pu. J. Phys. Chem. 132:(15)154104. https://10.1063/1.3382344
13. Besora, M.; Vidossich, P.; Lledós, A.; Ujaque, G.; Maseras, F., (2018) Calculation of Reaction Free Energies in Solution: A Comparison of Current Approaches. J. Phys. Chem. A 122:(5)1392-1399. https://10.1021/acs.jpca.7b11580
14. Luchini, G.; Alegre-Requena, J. V.; Funes-Ardoiz, I.; Paton, R. S., (2020) GoodVibes: Automated thermochemistry for heterogeneous computational chemistry data. F1000Research 9:(291)291.
15. Pedregal, J. R. G.; Funes-Ardoiz, I.; Sciortino, G.; Sánchez-Aparicio, J. E.; Ujaque, G.; Lledós, A.; Maréchal, J. D.; Maseras, F., (2019) GARLEEK: Adding an extra flavor to ONIOM. J. Comput. Chem. 40:(2)381-386. https://10.1002/jcc.25612
16. Chung, L. W.; Sameera, W. M. C.; Ramozzi, R.; Page, A. J.; Hatanaka, M.; Petrova, G. P.; Harris, T. V.; Li, X.; Ke, Z.; Liu, F.; Li, H.-B.; Ding, L.; Morokuma, K., (2015) The ONIOM Method and Its Applications. Chem. Rev. 115:(12)5678-5796. https://10.1021/cr5004419
17. Thiel, W., (2014) Semiempirical quantum–chemical methods. WIREs Comput. Mol. Sci. 4:(2)145-157. https://10.1002/wcms.1161
18. Christensen, A. S.; Kubař, T.; Cui, Q.; Elstner, M., (2016) Semiempirical Quantum Mechanical Methods for Noncovalent Interactions for Chemical and Biochemical Applications. Chem. Rev. 116:(9)5301-5337. https://10.1021/acs.chemrev.5b00584
19. Grimme, S.; Bannwarth, C.; Shushkov, P., (2017) A Robust and Accurate Tight-Binding Quantum Chemical Method for Structures, Vibrational Frequencies, and Noncovalent Interactions of Large Molecular Systems Parametrized for All spd-Block Elements (Z = 1–86). J. Chem. Theory Comput. 13:(5)1989-2009. https://10.1021/acs.jctc.7b00118

20. Stewart, J. J. P., (2013) Optimization of parameters for semiempirical methods VI: more modifications to the NDDO approximations and re-optimization of parameters. J. Mol. Model. 19:(1)1-32. https://10.1007/s00894-012-1667-x
21. Tomasi, J.; Mennucci, B.; Cammi, R., (2005) Quantum Mechanical Continuum Solvation Models. Chem. Rev. 105:(8)2999-3094. https://10.1021/cr9904009
22. Marenich, A. V.; Cramer, C. J.; Truhlar, D. G., (2009) Universal Solvation Model Based on Solute Electron Density and on a Continuum Model of the Solvent Defined by the Bulk Dielectric Constant and Atomic Surface Tensions. J. Phys. Chem. B 113:(18)6378-6396. https://10.1021/jp810292n
23. Klamt, A.; Schüürmann, G., (1993) COSMO: a new approach to dielectric screening in solvents with explicit expressions for the screening energy and its gradient. J. Chem. Soc., Perkin Trans. (5)799-805. https://10.1039/P29930000799
24. Besora, M.; Braga, A. A. C.; Ujaque, G.; Maseras, F.; Lledós, A., (2011) The importance of conformational search: a test case on the catalytic cycle of the Suzuki–Miyaura cross-coupling. Theor. Chem. Acc. 128:(4)639-646. https://10.1007/s00214-010-0823-6
25. Seminario, J. M., (1996) Calculation of intramolecular force fields from second-derivative tensors. Int. J. Quantum Chem. 60:(7)1271-1277. https://doi:10.1002/(SICI)1097-461X(1996)60:7<1271::AID-QUA8>3.0.CO;2-W
26. Li, P.; Merz, K. M., (2016) MCPB.py: A Python Based Metal Center Parameter Builder. J. Chem. Inf. Model. 56:(4)599-604. https://10.1021/acs.jcim.5b00674
27. Zheng, S.; Tang, Q.; He, J.; Du, S.; Xu, S.; Wang, C.; Xu, Y.; Lin, F., (2016) VFFDT: A New Software for Preparing AMBER Force Field Parameters for Metal-Containing Molecular Systems. J. Chem. Inf. Model. 56:(4)811-818. https://10.1021/acs.jcim.5b00687
28. Vidossich, P.; Lledós, A.; Ujaque, G., (2016) First-Principles Molecular Dynamics Studies of Organometallic Complexes and Homogeneous Catalytic Processes. Acc. Chem. Res. 49:(6)1271-1278. https://10.1021/acs.accounts.6b00054
29. Marx, D.; Hutter, J., *Ab Initio Molecular Dynamics: Basic Theory and Advanced Methods*. Cambridge University Press: Cambridge, 2009.
30. Car, R.; Parrinello, M., (1985) Unified Approach for Molecular Dynamics and Density-Functional Theory. Phys. Rev. Lett. 55:(22)2471-2474. https://10.1103/PhysRevLett.55.2471
31. Vidossich, P.; Magistrato, A., (2014) QM/MM Molecular Dynamics Studies of Metal Binding Proteins. Biomolecules 4:(3)616.
32. Besora, M.; Maseras, F., (2018) Microkinetic modeling in homogeneous catalysis. WIREs Comput. Mol. Sci. 8:(6)e1372. https://https://doi.org/10.1002/wcms.1372
33. Jaraíz, M., (2020) DFT-based microkinetic simulations: a bridge between experiment and theory in synthetic chemistry. New Directions in the Modeling of Organometallic Reactions 81-105.
34. Weinhold, F., Natural Bond Orbital Methods. In *Encyclopedia of Computational Chemistry*, 1998.
35. Bader, R. F., (1985) Atoms in molecules. Acc. Chem. Res. 18:(1)9-15.
36. Fernández, I.; Bickelhaupt, F. M., (2014) The activation strain model and molecular orbital theory: understanding and designing chemical reactions. Chem. Soc. Rev. 43:(14)4953-4967. https://10.1039/C4CS00055B
37. Daver, H.; Harvey, J. N.; Rebek, J.; Himo, F., (2017) Quantum Chemical Modeling of Cycloaddition Reaction in a Self-Assembled Capsule. J. Am. Chem. Soc. 139:(43)15494-15503. https://10.1021/jacs.7b09102
38. Sciortino, G.; Lledós, A.; Vidossich, P., (2019) Bonding rearrangements in organometallic reactions: from orbitals to curly arrows. Dalton Trans. 48:(42)15740-15752. https://10.1039/C9DT03063H
39. Zhang, J.-X.; Sheong, F. K.; Lin, Z., (2018) Unravelling Chemical Interactions with Principal Interacting Orbital Analysis. Chem. Eur. J. 24:(38)9639-9650. https://https://doi.org/10.1002/chem.201801220
40. Zhang, J.-X.; Sheong, F. K.; Lin, Z., (2020) Principal interacting orbital: A chemically intuitive method for deciphering bonding interaction. WIREs Comput. Mol. Sci. 10:(6)e1469. https://https://doi.org/10.1002/wcms.1469
41. Contreras-García, J.; Johnson, E. R.; Keinan, S.; Chaudret, R.; Piquemal, J.-P.; Beratan, D. N.; Yang, W., (2011) NCIPLOT: A Program for Plotting Noncovalent Interaction Regions. J. Chem. Theory Comput. 7:(3)625-632. https://10.1021/ct100641a
42. Funes-Ardoiz, I.; Maseras, F., (2018) Oxidative Coupling Mechanisms: Current State of Understanding. ACS Catal. 8:(2)1161-1172. https://10.1021/acscatal.7b02974

43. Ueura, K.; Satoh, T.; Miura, M., (2007) Rhodium- and Iridium-Catalyzed Oxidative Coupling of Benzoic Acids with Alkynes via Regioselective C−H Bond Cleavage. J. Org. Chem. 72:(14)5362-5367. https://10.1021/jo070735n
44. Ueura, K.; Satoh, T.; Miura, M., (2007) An Efficient Waste-Free Oxidative Coupling via Regioselective C−H Bond Cleavage: Rh/Cu-Catalyzed Reaction of Benzoic Acids with Alkynes and Acrylates under Air. Org. Lett. 9:(7)1407-1409. https://10.1021/ol070406h
45. Funes-Ardoiz, I.; Maseras, F., (2016) Cooperative Reductive Elimination: The Missing Piece in the Oxidative-Coupling Mechanistic Puzzle. Angew. Chem. Int. Ed. 55:(8)2764-2767. https://https://doi.org/10.1002/anie.201510540
46. Funes-Ardoiz, I.; Maseras, F., (2018) Computational Characterization of the Mechanism for the Oxidative Coupling of Benzoic Acid and Alkynes by Rhodium/Copper and Rhodium/Silver Systems. Chem. Eur. J. 24:(47)12383-12388. https://https://doi.org/10.1002/chem.201800627
47. Rivada-Wheelaghan, O.; Comas-Vives, A.; Fayzullin, R. R.; Lledós, A.; Khusnutdinova, J. R., (2020) Dynamic PdII/CuI Multimetallic Assemblies as Molecular Models to Study Metal–Metal Cooperation in Sonogashira Coupling. Chem. Eur. J. 26:(53)12168-12179. https://https://doi.org/10.1002/chem.202002013
48. Martínez de Salinas, S.; Mudarra, Á. L.; Benet-Buchholz, J.; Parella, T.; Maseras, F.; Pérez-Temprano, M. H., (2018) New Vistas in Transmetalation with Discrete "AgCF3" Species: Implications in Pd-Mediated Trifluoromethylation Reactions. Chem. Eur. J. 24:(46)11895-11898. https://https://doi.org/10.1002/chem.201802586
49. Feng, W.; Wang, T.; Liu, D.; Wang, X.; Dang, Y., (2019) Mechanism of the Palladium-Catalyzed C(sp3)–H Arylation of Aliphatic Amines: Unraveling the Crucial Role of Silver(I) Additives. ACS Catal. 9:(8)6672-6680. https://10.1021/acscatal.9b01412
50. Wu, C.; McCollom, S. P.; Zheng, Z.; Zhang, J.; Sha, S.-C.; Li, M.; Walsh, P. J.; Tomson, N. C., (2020) Aryl Fluoride Activation through Palladium–Magnesium Bimetallic Cooperation: A Mechanistic and Computational Study. ACS Catal. 10:(14)7934-7944. https://10.1021/acscatal.0c01301
51. Yoshikai, N.; Matsuda, H.; Nakamura, E., (2009) Hydroxyphosphine Ligand for Nickel-Catalyzed Cross-Coupling through Nickel/Magnesium Bimetallic Cooperation. J. Am. Chem. Soc. 131:(27)9590-9599. https://10.1021/ja903091g
52. Yoshikai, N.; Mashima, H.; Nakamura, E., (2005) Nickel-Catalyzed Cross-Coupling Reaction of Aryl Fluorides and Chlorides with Grignard Reagents under Nickel/Magnesium Bimetallic Cooperation. J. Am. Chem. Soc. 127:(51)17978-17979. https://10.1021/ja056327n
53. Bhaskararao, B.; Singh, S.; Anand, M.; Verma, P.; Prakash, P.; C, A.; Malakar, S.; Schaefer, H. F.; Sunoj, R. B., (2020) Is silver a mere terminal oxidant in palladium catalyzed C–H bond activation reactions? Chem. Sci. 11:(1)208-216. https://10.1039/C9SC04540F
54. Wang, J.; Zhan, L.; Wang, G.; Wei, Y.; Shi, M.; Zhang, J., (2020) Pd-Promoted cross coupling of iodobenzene with vinylgold via an unprecedented phenyl transmetalation from Pd to Au. Chem. Commun. 56:(46)6213-6216. https://10.1039/D0CC02645J
55. Fromm, A.; van Wüllen, C.; Hackenberger, D.; Gooßen, L. J., (2014) Mechanism of Cu/Pd-Catalyzed Decarboxylative Cross-Couplings: A DFT Investigation. J. Am. Chem. Soc. 136:(28)10007-10023. https://10.1021/ja503295x
56. Deolka, S.; Rivada-Wheelaghan, O.; Aristizábal, S. L.; Fayzullin, R. R.; Pal, S.; Nozaki, K.; Khaskin, E.; Khusnutdinova, J. R., (2020) Metal–metal cooperative bond activation by heterobimetallic alkyl, aryl, and acetylide PtII/CuI complexes. Chem. Sci. 11:(21)5494-5502. https://10.1039/D0SC00646G
57. Zhang, H.; Hatzis, G. P.; Dickie, D. A.; Moore, C. E.; Thomas, C. M., (2020) Redox chemistry and H-atom abstraction reactivity of a terminal zirconium(iv) oxo compound mediated by an appended cobalt(i) center. Chem. Sci. 11:(39)10729-10736. https://10.1039/D0SC04229C
58. Ye, J.; Cammarota, R. C.; Xie, J.; Vollmer, M. V.; Truhlar, D. G.; Cramer, C. J.; Lu, C. C.; Gagliardi, L., (2018) Rationalizing the Reactivity of Bimetallic Molecular Catalysts for CO2 Hydrogenation. ACS Catal. 8:(6)4955-4968. https://10.1021/acscatal.8b00803
59. Musgrave, C. B.; Zhu, W.; Coutard, N.; Ellena, J. F.; Dickie, D. A.; Gunnoe, T. B.; Goddard, W. A., (2021) Mechanistic Studies of Styrene Production from Benzene and Ethylene Using [(η2-C2H4)2Rh(μ-OAc)]2 as Catalyst Precursor: Identification of a Bis-RhI Mono-CuII Complex As the Catalyst. ACS Catal. 11:(9)5688-5702. https://10.1021/acscatal.1c01203
60. Kalek, M.; Himo, F., (2017) Mechanism and Selectivity of Cooperatively Catalyzed Meyer–Schuster Rearrangement/Tsuji–Trost Allylic Substitution. Evaluation of Synergistic Catalysis by Means of

Combined DFT and Kinetics Simulations. J. Am. Chem. Soc. 139:(30)10250-10266. https://10.1021/jacs.7b01931
61. Zamani, F.; Babaahmadi, R.; Yates, B. F.; Gardiner, M. G.; Ariafard, A.; Pyne, S. G.; Hyland, C. J. T., (2019) Dual Gold-Catalyzed Cycloaromatization of Unconjugated (E)-Enediynes. Angew. Chem. Int. Ed. 58:(7)2114-2119. https://https://doi.org/10.1002/anie.201810794